JOURNAL OF CATALYSIS **173,** 157–171 (1998)
ARTICLE NO. CA971910

CO_2 Reforming of CH_4 over Supported Pt Catalysts

Michael C. J. Bradford[1] and M. Albert Vannice[2]

Department of Chemical Engineering, Pennsylvania State University, University Park, Pennsylvania 16802-4400

Received April 24, 1997; revised September 23, 1997; accepted September 23, 1997

The kinetics of CO_2 reforming of CH_4 were studied over Pt supported on TiO_2, ZrO_2, Cr_2O_3, and SiO_2, and the catalysts were characterized using chemisorption, X-ray diffraction, diffuse reflectance infrared Fourier transform spectroscopy (DRIFTS), temperature-programmed hydrogenation (TPH), and temperature-programmed surface reaction. Although the Pt/SiO_2 and Pt/Cr_2O_3 catalysts deactivated significantly within 5 and 15 h onstream, respectively, the Pt/ZrO_2 and Pt/TiO_2 catalysts exhibited much higher stability even after 80 to 100 h onstream. TPH results with used catalysts showed that both Pt/ZrO_2 and Pt/TiO_2 have suppressed carbon deposition under reaction conditions. H_2 and CO chemisorption as well as DRIFTS provided evidence of metal–support interactions in the Pt/TiO_2 catalyst and indicated that large ensembles of Pt atoms, active for carbon deposition, are deactivated or destroyed by the presence of mobile TiO_x species. Activities for CO formation and CH_4 consumption on a turnover frequency basis were five times greater on Pt/TiO_2 compared with the other catalysts, suggesting that active sites for reforming are created in the Pt–TiO_x interfacial region. The kinetic behavior was explained well by a kinetic model recently proposed for supported Ni.

INTRODUCTION

The catalytic reforming of CH_4 with CO_2, rather than H_2O, for the production of synthesis gas is attractive industrially because it yields low H_2/CO product ratios which are preferable as feeds for Fischer–Tropsch synthesis reactions (1). Although conversion of CH_4 and CO_2 into fuels cannot in the long term ameliorate greenhouse gas emissions, CO_2–CH_4 reforming has shown promise in chemical energy transmission systems, such as the Solchem Process (2), the CSIRO/Pacific Power Project (3), and the CLEA Project (4). Regardless, environmentally friendly applications of CO_2–CH_4 reforming are a better alternative to reduce greenhouse gas emissions than the mass execution of ruminants (5), and some industrial processes that use CO_2 reforming, such as the Calcor Process (6) and the SPARG Process (7), are currently in operation.

All of the Group VIII metals, with the exception of Os, on a variety of supports have been studied as CO_2–CH_4 reforming catalysts (8–14), and Pt/Al_2O_3 (15–22), Pt/ZrO_2 (21, 22), Pt/MgO (23–25), Pt/TiO_2 (22), Pt/SiC (26), Pt/CeO_2 (27), $Pt/Ni/CeO_2$ (28), Pt/NaY (29), and Pt wire (30) have been previously investigated; however, no detailed analysis of the role of the support in the reaction kinetics of CO_2 reforming of CH_4 has been reported for Pt catalysts. There have been relatively few investigations of CO_2–CH_4 reforming over ZrO_2- and TiO_2-supported Pt, and use of either Cr_2O_3 or SiO_2 as a support for Pt has yet not been reported in the open literature. Thus, the primary purposes of this study were to elucidate the role of the support in catalytic behavior, to determine reaction kinetics, and to examine the coking resistance of supported Pt catalysts.

EXPERIMENTAL

Three supported Pt catalysts, sieved to a 120/70-mesh fraction (0.12–0.20 mm), were prepared via an incipient wetness technique by impregnating SiO_2 (Davison Grade 57), Cr_2O_3 (Aldrich), and TiO_2 (Degussa P-25) with $H_2PtCl_6 \cdot H_2O$ (Aldrich). The Pt/ZrO_2 catalyst (<120 mesh) used in this investigation was obtained from J. Lercher and was also prepared with an $H_2PtCl_6 \cdot H_2O$ precursor (22).

A reduction at 773 K was used with all catalysts. The first step of this pretreatment consisted of heating in 12 sccm hydrogen (WHSV = 14,000–29,000 $cm^3\ h^{-1}\ g^{-1}$) for 30 min at 423 K, followed by heating to 773 K and reducing in flowing hydrogen for 60 min. After cooling the catalyst in flowing H_2 to 723 K the catalyst was purged with flowing He (36 sccm) for 30 min. This procedure has been shown by numerous preceding studies to establish the "SMSI" state (31).

An Omnisorb 100CX VER 1F system was used to simultaneously obtain catalyst BET surface areas and pore size distributions. H_2 and CO chemisorption was measured on all catalysts at 300 K after the 773 K reduction using a stainless-steel volumetric apparatus to determine Pt surface atoms available via application of the dual-isotherm method (32). Because reduction of Pt/TiO_2 at 773 K is known to induce a metal–support interaction (MSI) state (31), additional isotherms were obtained at 300 K after

[1] Current address: Exxon Chemical Company, PO Box 4900, 4500 Bayway Drive, Baytown, TX 77522-4900.

[2] To whom correspondence should be addressed. Fax: (+1-814) 865-7846.

0021-9517/98 $25.00

reduction of Pt/TiO_2 at 473 K to better estimate the Pt dispersion and crystallite size in this catalyst.

X-ray diffraction (XRD), performed with either a Scintag VAX 3100 or a Rigaku Geigerflex system using filtered Cu$K\alpha$ radiation, was used to identify the bulk phases of the reduced catalyst samples. Pt reflections could be detected only for the 0.79% Pt/SiO_2 sample.

A high-temperature reactor system described previously (10) was used to determine catalyst activity. The amount of catalyst used during these experiments varied from 20 to 50 mg to maintain differential conditions, which were typically less than 6% CH_4 conversion. All activity tests were carried out under ca. 740 Torr absolute pressure, with a feed composition of $CO_2/CH_4/He = 1/1/1.8$ and a total feed flow rate of 20 sccm (WHSV = 38,000–52,000 $cm^3\ g^{-1}\ h^{-1}$) over the temperature range 673 to 723 K. The partial pressure dependencies were determined by maintaining 200 Torr of one reactant and varying the other reactant between approximately 40 and 400 Torr pressure while the balance of He was adjusted to maintain a total gas flow rate of 20 sccm. Thermodynamic equilibrium calculations were performed using ARL-SOLGASMIX (Release II) for comparative purposes (33).

Temperature-programmed hydrogenation (TPH) was used to investigate carbonaceous deposits on used catalyst samples. After termination of reaction, the catalyst was purged with He for 30 min, typically at 723 K, and then cooled slowly overnight to room temperature. The following day the temperature was ramped at a rate of 10 ± 1 K/min from 298 to 1073 K while a 50% mixture of H_2 in He was passed through the catalyst bed at ca. 740 Torr absolute pressure. Integration of the CH_4 evolution spectra, measured every 2 min with the on-line gas chromatograph, allowed for quantification of carbon deposition. During TPH no evidence of higher hydrocarbon formation was observed.

Temperature-programmed surface reaction (TPSR) was also used to investigate CO_2 reforming of CH_4 over Pt/TiO_2. After completion of the 773 K reduction procedure, the catalyst was purged with He at 723 K and cooled overnight to room temperature. The following day, the reduced Pt/TiO_2 catalyst was first exposed to 200 Torr of flowing CO_2 ($CO_2/He = 1/2.8$) at 300 K for 1 h and subsequently purged in flowing He until no gas-phase species were detected in the GC trace. The catalyst was then ramped at 10 ± 1 K/min to 1173 K in 200 Torr of flowing CH_4 ($CH_4/He = 1/2.8$) while the gas phase was sampled with the on-line GC every 2 min.

An N_2-purged FTIR spectrometer (Mattson Instruments, RS-10000) equipped with a diffuse reflectance infrared Fourier transform spectroscopy (DRIFTS) cell (Harrick Scientific, HVC-DR2) and a praying mantis mirror assembly (Harrick Scientific, DRA-2CO) was used to study CO and CO_2 adsorption, as well as CO_2–CH_4 reforming between 300 and 773 K. All spectra were obtained as an average of 1000 scans, except where noted, from 750 to 4000 cm^{-1} with a resolution of 4 cm^{-1}. To study irreversible CO adsorption at 300 K, the gas was made to flow over the catalyst at 300 K for 15 min, followed by a purge in a pure He/Ar mixture to remove gas-phase and reversibly adsorbed species. Both CO_2 adsorption (80 Torr) and CO_2–CH_4 reforming ($P_{CH_4} = P_{CO_2} \cong 80$ Torr) were studied in the presence of the gas-phase reactants.

RESULTS

DRIFT spectra of Pt/TiO_2, Pt/ZrO_2, Pt/Cr_2O_3, and Pt/SiO_2 after reduction at 773 K, referenced to the open beam, indicate that some hydroxyl groups remain following the pretreatment procedure, as hydroxyl bands are observable at 3615 and 3436 cm^{-1} on Cr_2O_3 and at 3736 cm^{-1} on SiO_2, as shown in Fig. 1. In the case of Pt/ZrO_2, two bands at 3729 and 3650 cm^{-1} can be assigned to linear OH on tetragonal ZrO_2 and bridging OH on monoclinic ZrO_2, respectively

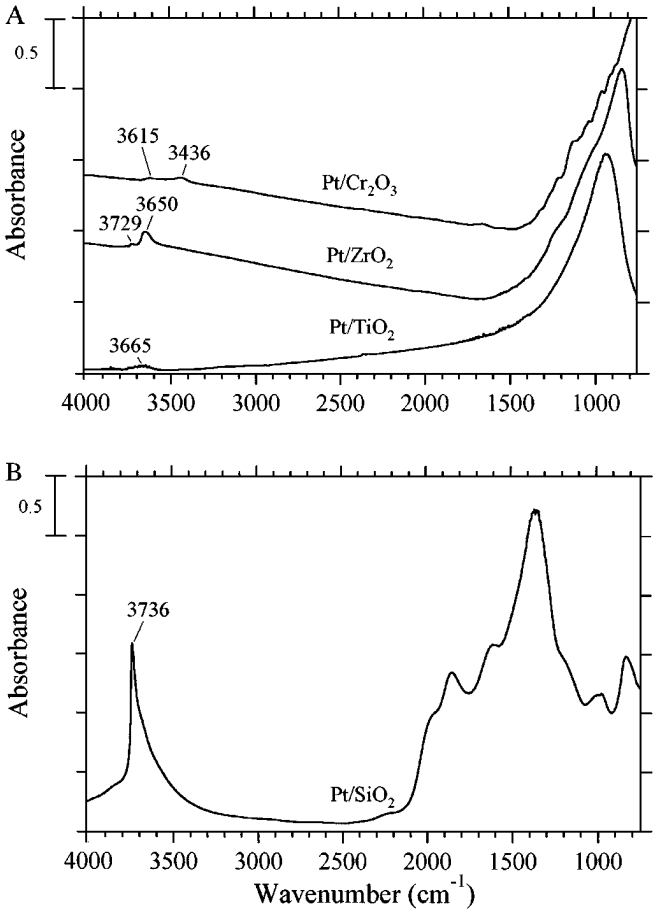

FIG. 1. DRIFT spectra of (A) Pt/TiO_2, Pt/ZrO_2, Pt/Cr_2O_3, and (B) Pt/SiO_2 after a 1-h reduction at 773 K referenced to the open beam background.

(34). Linear OH on monoclinic ZrO_2 should appear at ca. 3770 cm^{-1} (34, 35). The identification of this possible surface tetragonal phase by the observation of such OH groups must remain tentative, however, as both laser Raman and XRD spectra of the reduced Pt/ZrO_2 catalyst reveal only the bulk monoclinic structure. Nevertheless, the metastable tetragonal surface structure has been observed to exist (35).

DRIFT spectra of Pt/TiO_2 during reduction at 773 K were also obtained and referenced to the spectrum of the catalyst after only 1 min at 773 K. In this case, each spectrum was an average of only 100 scans. These spectra of Pt/TiO_2 during reduction at 773 K clearly show small losses at 3648 and 3608 cm^{-1}, due to removal of hydroxyl groups on the titania, and strong losses around 910 and 960 cm^{-1}, which are indicative of Ti–O bond cleavage (36) and TiO_x formation (Fig. 2).

A summary of the BET surface areas, pore radii, irreversible chemisorption uptakes, Pt dispersions, and Pt crystallite sizes determined for each catalyst is provided in Table 1. After a high-temperature reduction (HTR), H_2 chemisorption was completely suppressed and CO chemisorption was markedly decreased relative to that on Pt/TiO_2 reduced at 473 K. This type of behavior is routinely observed with TiO_2-supported metals after reduction at 773 K and is indicative of the SMSI state caused by the migration of TiO_x species onto the metal surface (31); consequently, these uptakes do not accurately measure dispersion, i.e., Pt_{surf}/Pt_{tot}. As mentioned previously, losses around 910 and 960 cm^{-1}, associated with titanium–oxygen bonds, during this reduction step are consistent with TiO_x formation (Fig. 2). In addition, a comparison of the DRIFT spectra in Fig. 3 of CO adsorbed on Pt/TiO_2 after

TABLE 1

BET Surface Areas (S), Mean Pore Radii (δ), Irreversible Chemisorption, Pt Dispersions (D), and Particle Sizes (d_s, d_v)

Catalyst[a]	T_r (K)[b]	S (m^2/g)	δ (Å)	Uptake ($\mu mol/g_{cat}$) CO[c]	Uptake ($\mu mol/g_{cat}$) H_2[d]	D (%)[e] CO	D (%)[e] H_2	d_s (nm)[f] CO	d_s (nm)[f] H_2
0.82% Pt/TiO_2	773	47	100	5.3 ± 0.9	0	12	0	—	—
	473	47	100	23.1 ± 0.9	15.9	55	75	2.0	1.5
0.31% Pt/ZrO_2	773	18	72	13.8 ± 2.4	6.5	87	82	1.3	1.4
0.75% Pt/Cr_2O_3	773	20	20	23.1 ± 0.9	7.0	60	37	1.9	3.1
0.79% Pt/SiO_2	773	271	90	10.6 ± 0.9	4.7	26	23	4.3	4.7

[a] Metal weight percentage determined by inductively coupled plasma spectrophotometry.
[b] Reduction temperature.
[c] Irreversible uptake at 100 Torr.
[d] Total uptake.
[e] Dispersions, i.e., Pt_{surf}/Pt_{tot}, calculated assuming $H_{ad}/Pt_{surf} = 1$ and $CO_{ad}/Pt_{surf} = 1$.
[f] Calculated from dispersion assuming spherical particles and using d_s (nm) $= 113/D$ (%).

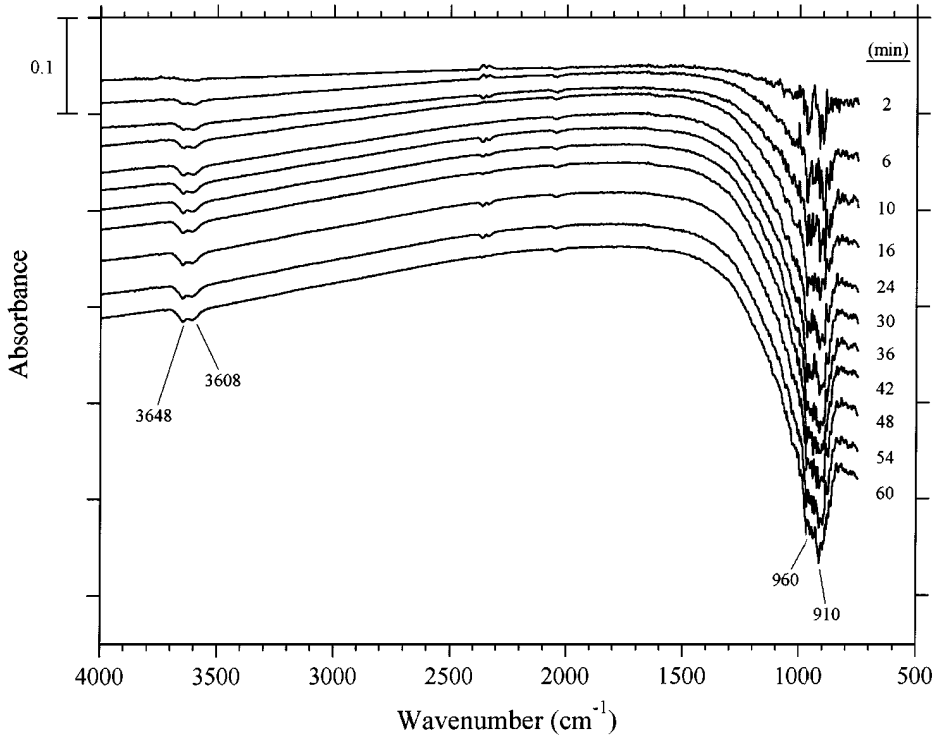

FIG. 2. Evolution of DRIFT spectra of Pt/TiO_2 during reduction at 773 K referenced to the initial spectrum of the catalyst at 773 K after 30 min reduction at 423 K and 1 min reduction at 773 K.

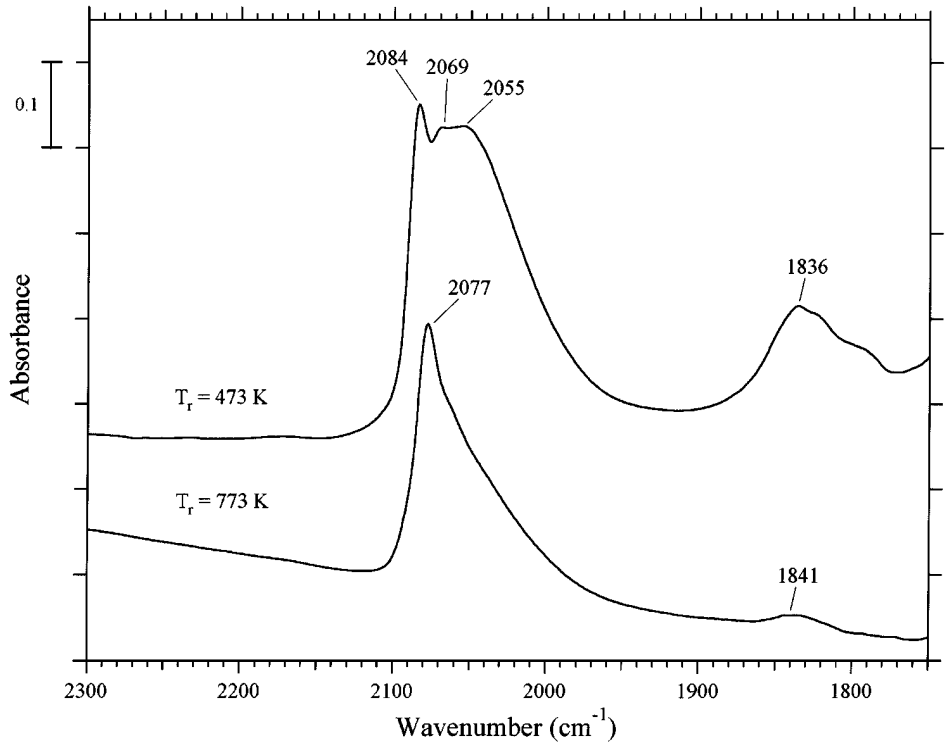

FIG. 3. Comparison of DRIFT spectra of CO adsorption on Pt/TiO_2 at 300 K after reduction at 473 and 773 K; the reference spectrum was that of the reduced catalyst at 300 K prior to CO admission.

reduction at either 473 or 773 K illustrates an ensemble effect caused by a TiO_x overlayer which reduces the population of linearly adsorbed CO near 2060 cm^{-1} and virtually eliminates bridge adsorption sites at 1836 cm^{-1}. Thus, to obtain a realistic estimate of the Pt particle size for the Pt/TiO_2 (HTR) catalyst in the presence of MSI, the value after reduction at 473 K was used because Baker *et al.* have shown using TEM that Pt particle sizes in Pt/TiO_2 after either a low- or a high-temperature reduction step are similar (37). Surface-weighted crystallite sizes determined from either H_2 or CO chemisorption were reasonably consistent for all other catalysts with the exception of Pt/Cr_2O_3. The latter discrepancy is most likely a result of some irreversible formate and carbonate formation on the Cr_2O_3 surface during CO adsorption (38), which caused an overestimate of the Pt dispersion.

From the XRD spectra of a number of Pt/TiO_2 catalyst samples, the mean composition of the titania (±SD), $74 \pm 4\%$ anatase, was calculated using a method described previously (10). Failure to observe any reduced forms of titania in the XRD spectrum of the reduced Pt/TiO_2 catalyst suggests that the Ti–O bond cleavage observed by DRIFTS during reduction (Fig. 2) is a surface-related phenomenon. XRD spectra of the Pt/ZrO_2, Pt/Cr_2O_3, and Pt/SiO_2 catalysts, both as prepared and after reduction at 773 K, reveal that the bulk structures are monoclinic (Baddeleyite), rhombohedral (Eskolaite), and amorphous, respectively. The absence of Pt reflections in the XRD spectra of reduced Pt/TiO_2, Pt/ZrO_2, and Pt/Cr_2O_3 indicate that the Pt is highly dispersed, in qualitative agreement with chemisorption results in Table 1, whereas a volume-weighted size of 11 nm was obtained for Pt/SiO_2.

To ensure that the measured rate data were free from mass transfer limitations, the Weisz criterion was evaluated (39) and satisfied for each catalyst, as all values were less than 0.3. In addition, reaction rates measured with Pt/ZrO_2 using either 0.12- to 0.2-mm or 0.3- to 0.6-mm particles were identical within experimental uncertainty, thus providing further evidence that the measured rates were free from diffusional effects. A comparison of the time-dependent activity shown in Fig. 4 for all supported catalysts reveals the following order of activity maintenance: $Pt/TiO_2 > Pt/ZrO_2 \gg Pt/Cr_2O_3 > Pt/SiO_2$. The Pt/SiO_2 and Pt/Cr_2O_3 catalysts exhibited high linear deactivation rates of $23 \pm 3\%$/h and $9.0 \pm 0.5\%$/h, respectively, presumably due to the rapid deposition of large amounts of inactive carbon, as discussed later. The initial deactivation rate of $1.4 \pm 0.8\%$/h for Pt/ZrO_2 was much lower than that observed for Pt/SiO_2, while the Pt/TiO_2 catalyst deactivated at a rate of only about 0.2%/h during the initial 100 h on-stream, at which time the run was ended.

During TPH experiments with Pt/ZrO_2 and Pt/TiO_2, CO and CO_2 evolution was observed at low temperatures. To further clarify the mechanism of CO formation during these

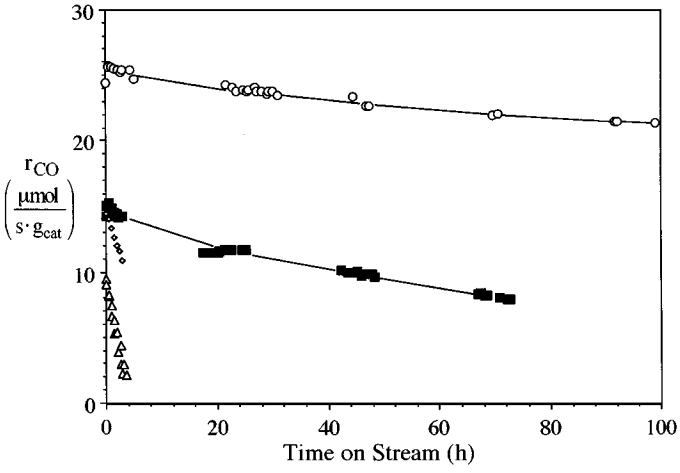

FIG. 4. Activity maintenance of (○) Pt/TiO_2, (■) Pt/ZrO_2, (△) Pt/Cr_2O_3, and (◇) Pt/SiO_2 at 723 K. Reaction conditions: $CH_4/CO_2/He = 1/1/1.8$, $P \approx 740$ Torr. All catalysts were reduced at 773 K.

experiments, TPH was performed in the DRIFTS cell with Pt/ZrO_2 after reaction for 1 h at 723 K and subsequent cooling in He to room temperature. By analyzing the gas effluent with on-line quadrupole mass spectroscopy, changes during TPH in the gas phase and on the catalyst surface could be observed simultaneously. After postreaction purging of the Pt/ZrO_2 catalyst in He and subsequent cooling to room temperature, DRIFT spectra indicated linear (2066 cm^{-1}) and bridged (1860 cm^{-1}) CO on Pt as well as hydroxyl (3750–3200 cm^{-1}) and carbonate (1300–1600 cm^{-1}) species on the ZrO_2 (Fig. 5). Initiation of the TPH resulted in immediate evolution of gas-phase CO, CO_2, and H_2O, and concomitant loss of surface hydroxyl and carbonate groups (Fig. 5). The coincidence of intensity maxima in Fig. 5 for adsorbed CO at 523 ± 50 K and gas-phase CO at 570 ± 10 K, as determined by separate TPH experiments, suggests that CO evolution during TPH is associated with the hydrogenation and/or decomposition of carbonate groups adsorbed on the support.

During TPH with Pt/Cr_2O_3 and Pt/SiO_2, no concomitant CO and CH_4 evolution was observed; thus, the high-temperature CH_4 formation at 1010 ± 10 K during TPH on these catalysts, as indicated in Fig. 6, is attributed to hydrogenation of surface carbon rather than hydrogenation of either adsorbed CO or carbonate groups. In contrast with the TPH spectra for Pt/Cr_2O_3 and Pt/SiO_2, a suppression of the 1010 ± 10 K CH_4 peak is observed with both Pt/TiO_2 and Pt/ZrO_2 (Fig. 6). Considering that the activities of Pt/TiO_2 and Pt/ZrO_2 are significantly more stable than that of either Pt/Cr_2O_3 or Pt/SiO_2 (Fig. 4), it seems likely that catalyst deactivation is associated with the presence of this highly inactive carbon deposit. Although no well-defined peaks are present in the TPH spectrum of the Pt/ZrO_2 catalyst, trace CH_4 formation began at about 500 K and continued

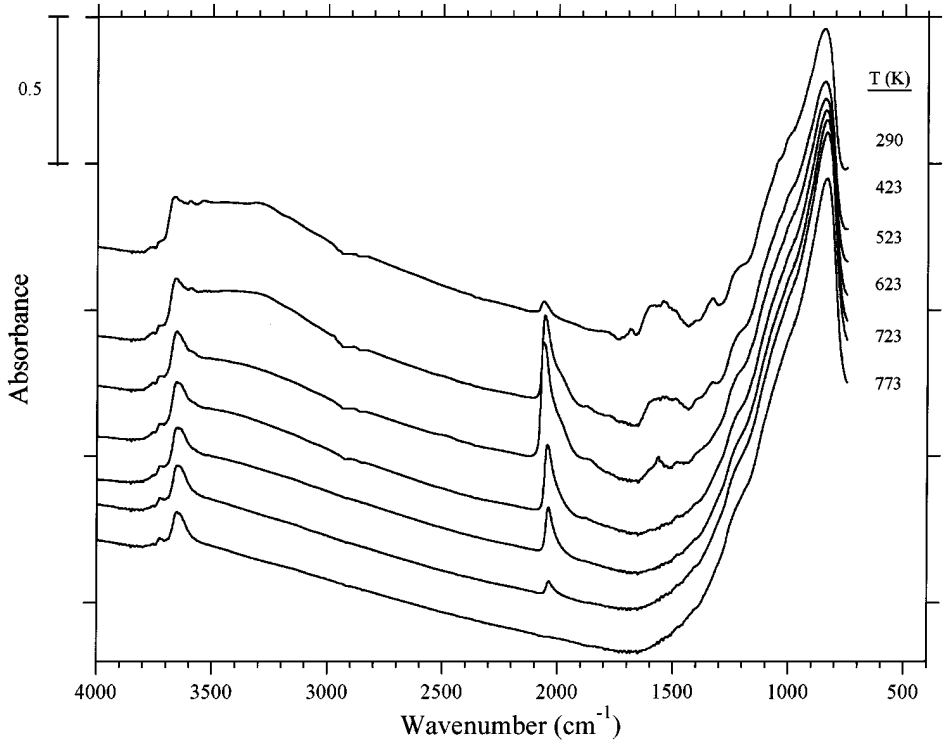

FIG. 5. DRIFT spectra during TPH with Pt/ZrO_2 referenced to an open beam background. Reaction conditions: $Ar/He/H_2 = 10/1/2.4$, $\beta = 10 \pm 1$ K/min.

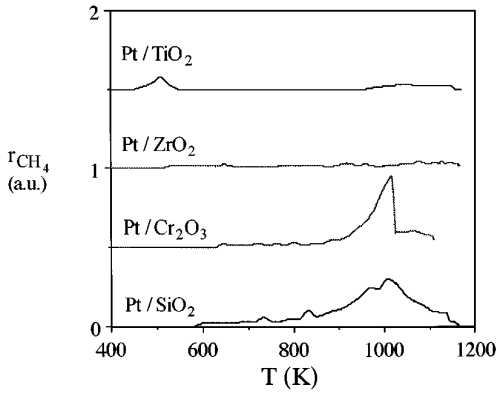

FIG. 6. TPH spectra for Pt/TiO_2, Pt/ZrO_2, Pt/Cr_2O_3, and Pt/SiO_2. Reaction conditions: $H_2/He = 1/1$, $P \approx 740$ Torr, $\beta = 10 \pm 1$ K/min. The samples were those used in Fig. 4.

for the remainder of the TPH experiment. Another interesting feature in the TPH spectra in Fig. 6 is a distinct CH_4 peak near 500 K with Pt/TiO_2. Because this peak occurs concomitantly with both CO and CO_2 evolution, it is very possible that this 500 K peak represents $CO-H_2$ methanation (40) rather than hydrogenation of a very reactive carbon deposit.

The amount of carbon deposited at 723 K after several hours onstream, as quantified by integration of the CH_4 formed during the TPH runs in Fig. 6, was normalized to surface Pt and gave C/Pt_{surf} ratios of 41 for Pt/SiO_2, 28 for Pt/Cr_2O_3, 9 for Pt/ZrO_2, and either 15 or 3 for Pt/TiO_2. The uncertainty in the value for Pt/TiO_2 reflects the choice of Pt surface area available after reduction at either 773 or 473 K (Table 1). Observance of CO adsorbed on the Pt surface in each catalyst under reaction conditions at 723 K indicates that the Pt surface is not entirely covered by carbon; thus these apparent supramonolayer carbon coverages must be due to accumulation of carbon on the support.

Measured reaction rates (μmol/s $\cdot$ g_{cat}) are normalized to the number of exposed Pt surface atoms as determined by chemisorption at 300 K to provide turnover frequencies (TOFs). Due to coverage by TiO_x species, which may be mobile under reaction conditions, the state of the Pt surface may be different than that of the metal surface postreduction prior to initiation of reaction; thus, to minimize complications in data interpretation, initial TOF values are reported. For Pt/TiO_2, initial TOFs for both CO production and CH_4 consumption, obtained after 30 min onstream, were calculated from the irreversible CO uptake after reduction at 773 K, whereas for the other catalysts, the TOFs were based on total H_2 uptakes after reduction at 773 K. These initial TOFs at 723 K were very similar for Pt/ZrO_2, Pt/Cr_2O_3, and Pt/SiO_2, while that for Pt/TiO_2 was about five times higher, as indicated in Table 2. A lower limit of the TOF for CO formation and CH_4 consumption on Pt/TiO_2 was obtained by normalizing reaction rates to the total H_2 uptake after reduction at 473 K when TiO_x species on the Pt surface are absent or minimal (Table 2); in this case, the TOF for Pt/TiO_2 is close to that of the other catalysts. However, the inhibition of carbon deposition illustrated in Fig. 6 is consistent with the presence of TiO_x species on the Pt surface; thus, the higher limit of the Pt/TiO_2 TOF value may be more reasonable. To correct for the severe deactivation of Pt/SiO_2 and Pt/Cr_2O_3, the reaction rates were normalized to a standard set of conditions which were monitored periodically throughout the duration of all experiments. Although the conversions of CH_4 and CO_2 at 723 K ranged from one-fifth to three-fifths of the calculated equilibrium conversions of 10.1 and 16.1%, respectively (see Table 2), H_2 partial pressure studies with Pt/TiO_2 indicated that in excess H_2, the reverse reaction, i.e., methanation, was negligible.

Activation energies for the consumption of CH_4 and CO_2 as well as the production of CO ($\pm$SD), H_2, and H_2O, obtained from Arrhenius plots such as those in Fig. 7, are also presented in Table 2. The apparent activation energies for Pt/TiO_2 and Pt/ZrO_2 are higher than those for Pt/Cr_2O_3 and Pt/SiO_2, and the apparent activation barrier for CH_4 consumption is 4 kcal/mol higher than that for CO_2

TABLE 2

Initial Catalyst Activity at 723 K and Apparent Activation Energies

Catalyst	Conversion (%)		Activity[a]			E_{app} (kcal/mol)				
	CH_4	CO_2	μmol CO/s $\cdot$ g_{cat}	TOF_{CO} (s^{-1})[b]	TOF_{CH_4} (s^{-1})[b]	CH_4	CO_2	CO	H_2	H_2O
Pt/TiO_2	6.0 ± 0.2	10.8 ± 0.5	26.0 ± 0.8	4.9 (0.82)[c]	1.8 (0.30)[c]	23	19	20.5 ± 0.4	32	18
Pt/ZrO_2	4.2 ± 0.1	7.8 ± 0.2	14.8 ± 0.3	1.1	0.39	24	20	21.6 ± 0.2	34	19
Pt/Cr_2O_3	3.7 ± 0.4	7.3 ± 0.5	15.2 ± 1.2	1.1	0.37	16	15	16	19	15
Pt/SiO_2	1.9 ± 0.4	3.4 ± 0.1	8.8 ± 0.8	0.94	0.34	15	19	17	[d]	[d]

[a] Initial activity after 30 min onstream.
[b] Calculated from the total H_2 uptake after reduction at 773 K, except where noted.
[c] Calculated from either irreversible CO uptake after reduction at 773 K (or total H_2 uptake after reduction at 473 K).
[d] Not possible to measure experimentally due to rapid catalyst deactivation.

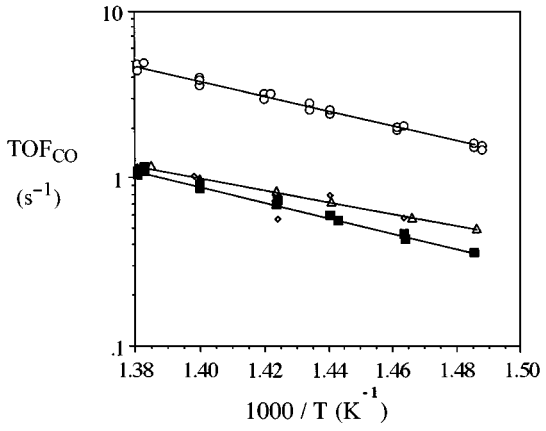

FIG. 7. Arrhenius plots of turnover frequencies for CO production (TOF_{CO}) on (○) Pt/TiO_2, (■) Pt/ZrO_2, (△) Pt/Cr_2O_3, and (◇) Pt/SiO_2. Reaction conditions: $CH_4/CO_2/He = 1/1/1.8$, $P \approx 740$ Torr.

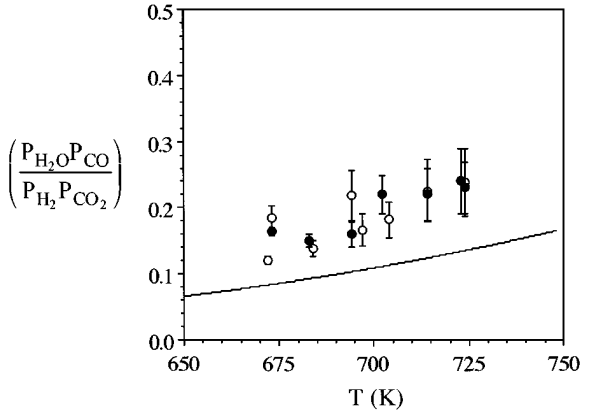

FIG. 9. Reverse water–gas shift pressure ratios, $P_{H_2O}P_{CO}/P_{H_2}P_{CO_2}$, for (○) Pt/TiO_2 and (●) Pt/ZrO_2 compared with the expected values at thermodynamic equilibrium (—). Reaction conditions: $CH_4/CO_2/He = 1/1/1.8$, $P \approx 740$ Torr.

consumption with both Pt/TiO_2 and Pt/ZrO_2. In the case of Pt/TiO_2, the higher apparent activation energy for CH_4 may be due to a geometric effect caused by TiO_x species on the Pt surface, as evidenced by suppressed chemisorption after reduction at 773 K (Table 1) and DRIFT spectra of adsorbed CO (Fig. 3). Also, the apparent activation energies for H_2 formation on all catalysts are greater than those for the formation of CO. This is presumably a result of the reverse water–gas shift (RWGS) reaction, which consumes H_2 to produce additional CO.

During the Arrhenius runs it was possible to monitor the H_2/CO product ratio to show that it increases concomitantly with reactant conversion, in qualitative agreement with thermodynamic equilibrium, as indicated in Fig. 8. The RWGS pressure ratio, ($P_{CO}P_{H_2O}/P_{CO_2}P_{H_2}$), determined for each catalyst during the activity runs, was very close to thermodynamic equilibrium over the temperature range investigated, as shown in Fig. 9. Error bars in the figure are due to uncertainty in the amount of H_2O. Thus, due to the strong influence of the RWGS reaction at these reaction temperatures and the low reactant conversions, the H_2/CO product ratios were always less than unity.

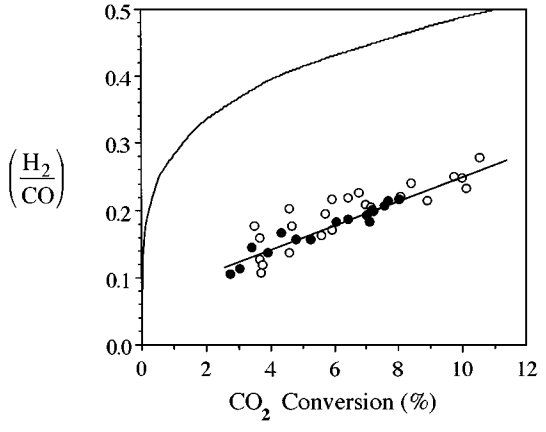

FIG. 8. H_2/CO product ratio as a function of CO_2 conversion for (○) Pt/TiO_2 and (●) Pt/ZrO_2 compared with the expected H_2/CO ratio at thermodynamic equilibrium (—). Reaction conditions: $CH_4/CO_2/He = 1/1/1.8$, $P \approx 740$ Torr.

The dependencies of the rates of H_2 and CO formation, as well as CH_4 and CO_2 consumption, on the partial pressures of CH_4 and CO_2 in the feed were determined under differential conditions for the Pt/TiO_2 and the Pt/ZrO_2 catalysts. The reaction orders for CH_4 and CO_2 were determined from a fit of the data to a power rate law of the general form

$$r_i = kP^a_{CH_4}P^b_{CO_2}, \qquad [1]$$

where i is the gas-phase species involved. Under differential conditions the gas-phase concentrations of H_2, CO, and H_2O are negligible; consequently, it is reasonable to exclude their partial pressures from Eq. [1] as a first approximation. Over the temperature range investigated, 673–723 K, the reaction orders varied very little within experimental error; thus for simplicity, mean values of the determined reaction orders (±SD) are reported in Table 3. The reaction orders for Pt/TiO_2 and Pt/ZrO_2 are quantitatively similar,

TABLE 3

Reaction Orders for Supported Pt Catalysts between 673 and 723 K

	$r_i = kP^a_{CH_4}P^b_{CO_2}$			
	Pt/TiO_2		Pt/ZrO_2	
i	a	b	a	b
CO_2	0.31 ± 0.01	0.28 ± 0.04	0.30 ± 0.05	0.21 ± 0.05
CH_4	0.28 ± 0.02	0.17 ± 0.04	0.30 ± 0.06	0.21 ± 0.16
CO	0.30 ± 0.01	0.24 ± 0.02	0.30 ± 0.01	0.20 ± 0.01
H_2	0.59 ± 0.04	-0.42 ± 0.17	0.50 ± 0.11	-0.37 ± 0.17
H_2O	0.24 ± 0.02	0.40 ± 0.04	0.26 ± 0.02	0.31 ± 0.05

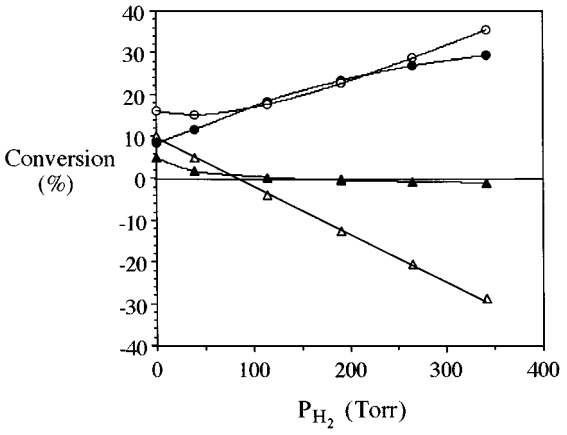

FIG. 10. Influence of H_2 in the feed on conversion: (○) CO_2 equilibrium conversion, (●) CO_2 experimental conversion, (△) CH_4 equilibrium conversion, (▲) CH_4 experimental conversion. Reaction conditions: $CH_4/CO_2/H_2/He = 1/1/n/1.8 - n$, $P \approx 740$ Torr.

which may indicate that the reaction mechanism is similar over both catalysts. In addition, the negative *b* values for H_2 production indicate consumption of H_2, presumably via the RWGS, as discussed previously. The influence of H_2 addition to the feedstream (with $P_{CH_4} = P_{CO_2} \cong 200$ Torr) is shown in Fig. 10 for the Pt/TiO_2 catalyst at 723 K. The immediate effect of high H_2 concentrations is to increase CO_2 conversion through the RWGS and to inhibit CH_4 consumption. Although thermodynamic calculations predict CH_4 formation at higher H_2 pressures, very little or no net methanation was observed over Pt/TiO_2 (negative conversion refers to the production of CH_4). Although this is in contrast to that observed previously with either Ni/MgO or Ni/TiO_2 (10), this is consistent with the observation that supported Ni is a better methanation catalyst than supported Pt (40).

To better understand the activation of CO_2 on the supported Pt catalysts, CO_2 adsorption was studied *in situ* at 723 K using DRIFTS. After reduction at 773 K in H_2, the catalyst was cooled to 723 K and purged for 30 min in an Ar/He mixture to remove surface hydrogen. Spectra were then obtained with CO_2 (80 Torr) flowing over the catalyst. In all cases, difference spectra were obtained by referencing to the freshly reduced catalyst prior to CO_2 admission. The bands of gas-phase CO_2 were removed from the spectra using appropriate subtraction procedures. Spectra following CO_2 adsorption on all four supported Pt catalysts revealed vibrations indicative of CO adsorbed on atop ($\eta = 1$) and bridged ($\eta = 2$) sites on Pt and possible monodentate carbonate species on the support, as shown in Fig. 11 and Table 4. Corresponding bands for bidentate carbonate should have a larger separation (34, 41). The bands observed at 1563 and 1357 cm^{-1} on Pt/Cr_2O_3 can be tentatively assigned to the $\nu_{as}(COO^-)$ and $\nu_s(COO^-)$ modes of surface carboxylate groups (41). It should be noted that the appearance of many overlapping bands in the carbonate region of the IR spectra for Pt/ZrO_2 and Pt/Cr_2O_3 makes unequivocal assignment of many bands difficult; nevertheless, a possible assignment to surface formate species is excluded because of the absence of C–H vibrations in the spectral region 2800–3000 cm^{-1}. Although the band at 1724 cm^{-1} on Pt/Cr_2O_3 has been assigned previously to a ν_3 mode of bidentate carbonate (38), corresponding bidentate bands at 1679 and 1280 cm^{-1} are absent from the spectra. Nevertheless, the 1724 cm^{-1} band is tentatively assigned to either a combination band or to the symmetric C=O stretch of some CO_x surface species. After a 20-min exposure of reduced

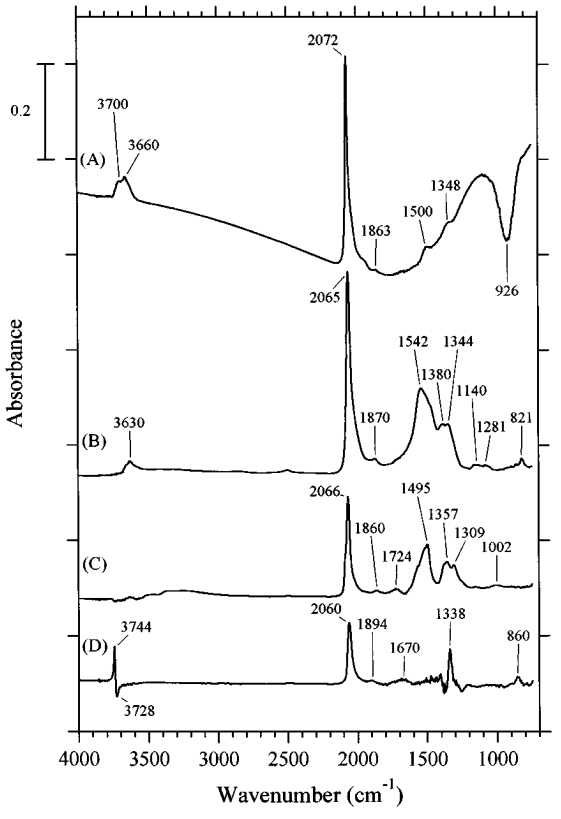

FIG. 11. DRIFT spectra of CO_2 adsorption (80 Torr) at 723 K on reduced (A) Pt/TiO_2, (B) Pt/ZrO_2, (C) Pt/Cr_2O_3, and (D) Pt/SiO_2. The reference spectrum was that of the catalyst prior to CO_2 admission.

TABLE 4

Wavenumbers of Species Observed during CO_2 Adsorption at 723 K

Catalyst	CO		Monodentate carbonate		
	$\nu_{\eta=1}$(C–O)	$\nu_{\eta=2}$(C–O)	$\nu_{as}(COO^-)$	$\nu_s(COO^-)$	ν(C–O)
Pt/TiO_2	2072	1863	1500	1348	—
Pt/ZrO_2	2065	1870	1542	1344	1081
Pt/Cr_2O_3	2066	1860	1512–1495	1309	1002
Pt/SiO_2	2060	1894	—	—	—

Pt/SiO_2 to CO_2, bands at 860, 1338, 1670, and 3744 cm^{-1} appeared with a loss at 3728 cm^{-1}, suggesting an interaction of CO_2 with isolated silanols on the SiO_2 surface to possibly form bicarbonate species, most likely with the low-level impurities (Na, Fe, Ca) in the silica used; however, this assignment is not definitive. In addition, the formation of hydroxyl groups on Pt/TiO_2 and Pt/ZrO_2 after CO_2 adsorption indicates that hydrogen atoms were present on the support following purging at 723 K. The formation of stable Zr^{n+}–H (42) and Ti^{n+}–H (43) species at exposed Lewis acid centers following exposure to H_2 has been previously reported in the literature.

The large loss observed near 926 cm^{-1} during CO_2 adsorption on Pt/TiO_2 was also observed during reduction at 773 K (Fig. 2) and is thus attributed to the rupture of surface titanium–oxygen bonds. Thus, the interaction of CO_2 with the reduced Pt/TiO_2 surface at 723 K is suggested to proceed via dissociative adsorption in the metal–support interfacial region, i.e.,

$$CO_2 + * + \begin{matrix} & O & \\ Ti & & Ti \end{matrix} \rightarrow CO* + \begin{matrix} O & & O \\ | & & | \\ Ti & & Ti \end{matrix}, \qquad [2]$$

where $*$ is a Pt site, and nondissociative adsorption on the titania surface, i.e.,

$$CO_2 + \begin{matrix} & O & \\ Ti & & Ti \end{matrix} \rightarrow \begin{matrix} & O & O \\ & \diagdown & \diagup \\ & & C \\ & \diagup & \diagdown \\ Ti & & Ti \end{matrix}. \qquad [3]$$

After exposure of the catalyst to flowing CO_2 at 723 K, CO_2–CH_4 reforming was studied *in situ* at 723 K with equimolar amounts of CH_4 and CO_2. The vibrational modes of gas-phase CH_4 were removed from the spectra using appropriate subtraction procedures. The spectra obtained with Pt/TiO_2, Pt/ZrO_2, and Pt/Cr_2O_3 under reaction conditions, shown in Fig. 12, referenced to the spectra of the reduced catalysts at 723 K prior to gas admission, clearly indicate the formation of hydroxyl groups on the oxide supports (3700–3300 cm^{-1}) and an increase in the band intensities for adsorbed CO species. A very weak band due to gas-phase CO is also present at 2143 cm^{-1}. All bands associated with monodentate carbonate species (Table 4) adsorbed on the support surface decreased in intensity, suggesting that these species are either reactive in the presence of CH_4 or displaced by CH_4 adsorbing on the support. The intensity of the loss at 926 cm^{-1} that occurred during CO_2 adsorption on Pt/TiO_2 (see Fig. 11) was markedly decreased after introduction of CH_4, and subsequent experiments revealed that this feature at 926 cm^{-1} could be acquired, decreased, and subsequently reobtained in a cyclic manner by respectively passing CO_2, CO_2–CH_4, and then CO_2 over the catalyst (44). This suggests that after oxidation of the TiO_2 surface by CO_2 via Eq. [2], the original state of the TiO_2 surface may

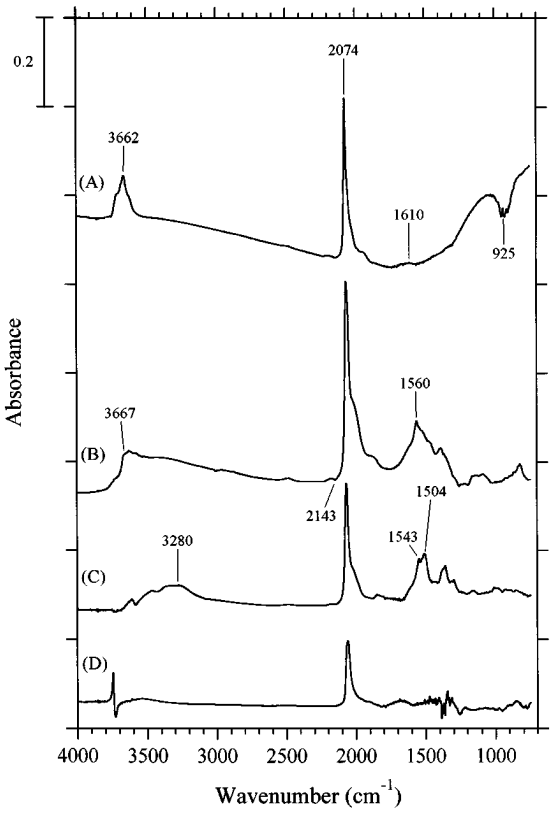

FIG. 12. DRIFT spectra of CO_2–CH_4 reforming at 723 K on reduced (A) Pt/TiO_2, (B) Pt/ZrO_2, (C) Pt/Cr_2O_3, and (D) Pt/SiO_2. The reference spectrum was that of the catalyst prior to gas admission. Reaction conditions: $P_{CH_4} = P_{CO_2} \approx 80$ Torr, balance Ar/He = 10/1.

be regained by reduction with CH_4; thus, a redox mechanism can occur on the TiO_2 surface under reaction conditions, most likely in the metal–support interfacial region. Spectra of Pt/Cr_2O_3 under reaction conditions also reveal the gradual disappearance of the weak band at 1724 cm^{-1}; however, the assignment of this band is uncertain so its significance is unclear at this time. Spectra obtained with Pt/SiO_2 under reaction conditions at 723 K revealed little about the catalyst surface, other than CO chemisorbed on Pt, represented by the band near 2074 cm^{-1} (Fig. 12).

During TPSR using CH_4 with Pt/TiO_2, two CO_2 desorption states occurred at about 350 and 590 K, as shown in Fig. 13. The two CO evolution maxima at 650 and 1130 K coincide precisely with the two observed maxima for H_2 evolution, also shown in Fig. 13, and the calculated H_2/CO ratio ($\pm$SD) above 600 K is 2.0 ± 0.4. Thus, the TPSR result suggests that CH_4 may reduce TiO_2 via the following stoichiometry:

$$xCH_4 + TiO_2 \rightarrow TiO_{2-x} + xCO + 2xH_2. \qquad [4]$$

Fancheng *et al.* have shown via XPS that CH_4 adsorption on reduced TiO_2 at 300 K results in the formation of both CH_x and CH_xO species (45); presumably, CH_xO species

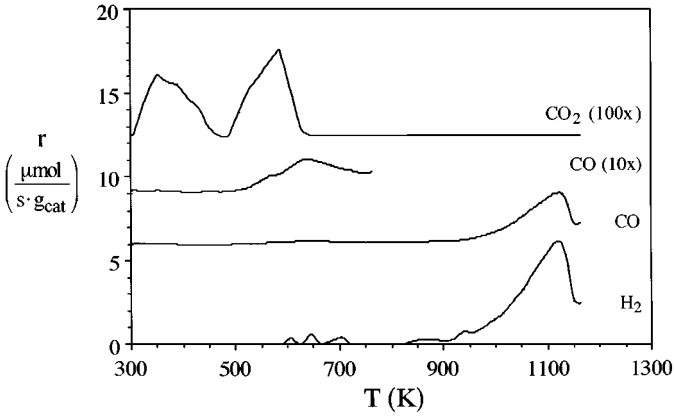

FIG. 13. CO_2 desorption and CO and H_2 formation during TPSR with reduced Pt/TiO_2. Reaction conditions: $CH_4/He = 1/2.8$, $P \approx 740$ Torr, $\beta = 10 \pm 1$ K/min.

may decompose at high temperatures to yield H_2 and CO. Analysis of CO formation during TPSR indicated that TiO_2 was reduced to $TiO_{1.7}$, and XRD analysis of the used sample after air exposure identified bulk rutile and Ti_9O_{17} phases, qualitatively verifying this analysis. No reflections due to anatase were present due to the anatase–rutile phase transformation above 773 K (46). Although many other reflections with *d* spacings less than 2 Å were identified in the XRD spectrum of this used Pt/TiO_2 catalyst, they could not be assigned to any of the known Ti_nO_{2n-1} Magneli phases; nevertheless, their presence is indicative of deeply reduced TiO_x phases.

DISCUSSION

Inactive carbon can originate during CO_2 reforming of CH_4 from either CO disproportionation,

$$2CO + * \leftrightarrow CO_2 + C*, \quad [5]$$

or CH_4 decomposition,

$$CH_4 + * \leftrightarrow C* + 2H_2. \quad [6]$$

Yu *et al.* observed that carbon accumulation on a Pt wire at CO_2–CH_4 reforming temperatures above 1273 K, which occurred for CH_4/CO_2 ratios larger than about 2.7, could be eliminated by addition of either H_2O or O_2 to the feed, presumably due to steam gasification or oxidation of the surface carbon (30). Although both Qin and Lapszewicz (24) and Rostrup-Nielsen and Bak Hansen (23) have reported carbon formation on Pt/MgO, the latter authors attributed the formation of whisker carbon to an Fe impurity. In this investigation, a comparison of the TPH results for the used catalysts (Fig. 6) indicated that both Pt/TiO_2 and Pt/ZrO_2 exhibit suppressed carbon deposition during CO_2–CH_4 reforming. It is important to understand why. As there is insufficient information to ascertain the predominant route to carbon formation over supported Pt, it is prudent to consider that both carbon formation reactions may participate. The possibility of Pt/TiO_2 and Pt/ZrO_2 deactivation due to gradual sintering of the Pt particles is excluded based on XRD spectra of the used Pt catalysts (44) and the results of Bitter *et al.* (22). The activity maintenance of the Pt/TiO_2 catalyst in the present study was far superior to that obtained with the Pt/TiO_2 catalyst prepared by Bitter *et al.* (22). This is most likely attributable to the quite different pretreatment, although their reaction conditions were also different.

Some theoretical calculations indicate that CO dissociation on metal surfaces requires an ensemble size of four to five metal atoms (47); thus, it can be argued that the presence of a TiO_x overlayer on the Pt surface reduces the number of large ensembles of Pt atoms and therefore geometrically inhibits CO dissociation. This view is consistent with recent results reported for Ni/TiO_2 (10) and Ni/La_2O_3 (48). In the latter study, Zhang and Verykios used similar arguments based on CO chemisorption and TPD to attribute the high activity and stability of certain Ni/La_2O_3 catalysts to LaO_x species on the Ni surface (48). It is relatively straightforward to argue that decoration of large Pt ensembles by TiO_x species also inhibits CH_4 decomposition. Minot *et al.* (49) and Koster and van Santen (50) have studied adsorbed CH_x fragments on Pt(111) and Rh(111) using variations of the extended Hückel method. The consistent qualitative conclusion drawn from each of these investigations is that CH_x fragments are preferentially located at a site on the metal surface that completes its tetravalency; i.e., the decomposition of CH_4 into CH_x fragments ($1 \le x \le 3$) on Pt(111) and Rh(111) should follow the general stoichiometry

$$CH_{x+1}\text{–}(3-x)M + 2M \rightarrow CH_x\text{–}(4-x)M + H\text{–}M, \quad [7]$$

where M is a surface metal atom. This stoichiometry, which is also valid for $x = 0$ provided that the metal surface in question has fourfold sites such as Pt(100), clearly implies that stepwise decomposition of CH_4 on Pt requires concomitant occupation of higher coordination sites. The presence of TiO_x overlayers on the Pt surface decreases the concentration of these large ensembles of Pt atoms and therefore inhibits complete CH_4 dissociation.

The reasons for the stability of Pt/ZrO_2, however, are less clear. Recently, van Keulen has shown using TGA that Pt/ZrO_2 inhibits both CO disproportionation and CO reduction (51), and Seshan *et al.* have used DSC/TGA to show that a 1.1% Pt/ZrO_2 catalyst exhibited little or no carbon formation during CO_2–CH_4 reforming after 500 h onstream at 853 K (21). Considering available literature data, it seems plausible that the higher stability and coking resistivity of Pt/ZrO_2 may be due to strong $Pt\text{–}Zr^{n+}$ interactions. The results of Roberts and Gorte for submonolayer Pt coverages on $ZrO_2(100)$ indicate that ZrO_2 influences the Pt surface,

presumably via a strong Zr^{n+}–Pt interaction, to alter Pt particle morphology and to lower the CO desorption barrier (52). In the absence of any detailed microscopic evidence, the role of Pt structure in our Pt/ZrO_2 catalyst is uncertain; however, if the highly dispersed Pt crystallites are preferentially located at Lewis acid sites on the oxide surface, as suggested by Masai *et al.* (19) and Roberts and Gorte (52), and Lewis acid sites on the support are the active sites for carbon deposition, as suggested by Bitter *et al.* (22), then the higher stability and coking resistivity of Pt/ZrO_2 may be due to strong $Pt–Zr^{n+}$ interactions which block active sites for carbon deposition. As noted previously, the ratios of deposited carbon atoms to surface Pt atoms ranged from 9 for Pt/ZrO_2 and Pt/TiO_2 to 41 for Pt/SiO_2, thus indicating the possibility of significant carbon formation on the support itself under reaction conditions. It is possible that a strong $Pt–Zr^{n+}$ interaction results in the formation of ZrO_x species on the Pt surface that function analogously to TiO_x species. Van Keulen has shown using HRTEM that ZrO_x species decorate the Pt surface after reduction at 1073 K (51); however, our chemisorption results indicate a high degree of Pt dispersion after reduction at 773 K, and it is unclear as to whether or not this MSI can occur at lower reduction temperatures. Nevertheless, the possibility cannot be excluded.

Some groups have speculated that increased Lewis basicity on the catalyst surface decreases carbon deposition during CO_2–CH_4 reforming via the reverse CO disproportionation reaction (53). Philipp and Fujimoto (54) have reported that the wavenumber difference of the symmetric and asymmetric stretching bands for surface carbonates, $\Delta\nu = \nu_{as} - \nu_s$, should decrease as the Lewis basicity of the surface increases. From the wavenumbers of monodentate carbonate on TiO_2, ZrO_2, and Cr_2O_3 obtained during the CO_2 adsorption studies at 723 K (Table 4), the calculated $\Delta\nu$ values for TiO_2, ZrO_2, and Cr_2O_3 are 152, 198, and 186–203 cm^{-1}, respectively, implying that after reduction at 773 K in hydrogen, the order of support basicity is $TiO_2 > ZrO_2 \approx Cr_2O_3$. These values of $\Delta\nu$ a priori predict carbon deposition during reaction to be in the order $Pt/TiO_2 < Pt/ZrO_2 \approx Pt/Cr_2O_3$; however, this prediction is in disagreement with both the observed catalyst stabilities and the TPH results for Pt/ZrO_2 and Pt/Cr_2O_3. Thus catalyst basicity, at least as measured by $\Delta\nu$, does not seem to correlate well with carbon deposition during CO_2–CH_4 reforming over supported Pt.

The TOFs are very similar for Pt/ZrO_2, Pt/Cr_2O_3, and Pt/SiO_2, while that for Pt/TiO_2 is five times higher based on CO adsorption after reduction at 773 K, although it is similar to the others when based on the Pt surface atoms available after reduction at 473 K. In view of this limited influence of the support on specific activity, it should be mentioned that Bitter *et al.* reported that the initial TOFs for CO_2 consumption at 875 K on Pt/TiO_2, Pt/ZrO_2, and Pt/Al_2O_3 were all approximately 3.5 s^{-1} (22). Although their TOFs at 875 K are of the same order of magnitude as our TOFs at only 723 K, the difference between our results and those of Bitter *et al.* (22) may be due to their higher reduction temperature of 1125 K, which markedly reduced Pt dispersion; i.e., there is evidence to indicate that CO_2–CH_4 reforming may be structure sensitive (44). The TOFs for CO production in Table 2 appear somewhat higher than those reported previously for Pt/Al_2O_3 and Pt/MgO (15, 23). Although few investigators have reported apparent activation energies for CO_2 reforming of CH_4 over supported Pt, the available values from the literature listed in Table 5 for Pt/Al_2O_3, Pt/ZrO_2, and Pt/MgO are both lower and higher than those obtained in this investigation. Nevertheless, it is noteworthy that in Table 5 the apparent activation energies for CH_4 consumption are higher than those for CO_2 consumption, in agreement with our results.

TABLE 5

Literature Values for Apparent Activation Energies with Pt Catalysts

Catalyst	E_{app} (kcal/mol)			Reference
	CH_4	CO_2	CO	
1.1% Pt/ZrO_2	15	14	15	(21)
1.1% Pt/Al_2O_3	14	13	—	(21)
2% Pt/Al_2O_3	15.1 ± 0.3	12.5 ± 0.4	—	(15)
0.9% Pt/MgO	35	—	—	(23)
0.5% Pt/MgO	33	—	—	(24)

After a thorough analysis of data available in the literature and numerous reaction models, the following generalized reaction sequence was previously proposed for the CO_2 reforming of CH_4 over supported Ni catalysts (10, 44):

$$\{1\} \quad CH_4 + * \underset{k_{-1}}{\overset{k_1}{\rightleftarrows}} CH_x* + ((4-x)/2)H_2,$$

$$\{2\} \quad 2\left[CO_2 + * \overset{K_2}{\rightleftharpoons} CO_2*\right],$$

$$\{3\} \quad H_2 + 2* \overset{K_3}{\rightleftharpoons} 2H*,$$

$$\{4\} \quad 2\left[CO_2* + H* \overset{K_4}{\rightleftharpoons} CO* + OH*\right],$$

$$\{5\} \quad OH* + H* \overset{K_5}{\rightleftharpoons} H_2O + 2*,$$

$$\{6\} \quad CH_x* + OH* \overset{K_6}{\rightleftharpoons} CH_xO* + H*,$$

$$\{7\} \quad CH_xO* \overset{k_7}{\rightarrow} CO* + (x/2)H_2,$$

$$\{8\} \quad 3\left[CO* \overset{1/K_8}{\rightleftharpoons} CO + *\right].$$

This sequence corresponds to the overall reaction stoichiometry

$$CH_4 + 2CO_2 \rightarrow H_2 + H_2O + 3CO. \quad [8]$$

It should be noted that the first step in the kinetic model, CH_4 adsorption and dissociation to a CH_x fragment, is a simplification of Eq. [7] in which any geometric constraint associated with precisely defined adsorption sites is removed to simplify the mathematical modeling. Nevertheless, formation of CH_x species is supported by previous studies, with the particular species formed having little influence on the derived rate expression (10).

Although some investigators have used pulsed CH_4 decomposition experiments at elevated temperatures (973 K) to show that pure CH_4 in an inert atmosphere decomposes stoichiometrically to C and $2H_2$ (55), pulsed CH_4 adsorption on Pt/Al_2O_3 at 773 K (15), the D_2–CH_4 exchange reaction on Rh/MgO (24), and CO_2 reforming of CH_4/CD_4 over Ni/SiO_2 (56) reveal a distribution of CH_x fragments on the catalyst surface. Although Kroll *et al*. have suggested that Ni_3C is the active phase during reaction (57), Osaki *et al*. have determined that the reactivity of surface carbon ($x = 0$) on supported Ni is lower than that of CH_x species under reforming conditions and concluded that it is only a minor reactive intermediate (58). The reversible CH_4 adsorption and dissociation step proposed in our model is supported by the effect of H_2 addition to the feed gas (Fig. 10), which showed that the CH_4 consumption rate was reversible and was not at thermodynamic equilibrium.

Although it has been suggested that adsorbed O atoms promote CH_4 dissociation (15), bond order conservation Morse potential (BOC-MP) calculations indicate that the activation energies for O-assisted CH_4 dissociation are higher than those for unassisted CH_4 dissociation on both Ni (59) and Pt (44) surfaces. Although TPSR experiments indicated that either CH_4 or CH_x activation by oxygen species on the support surface can occur, the rate of activation is much less than that in the presence of CO_2. Thus, step {1} in the proposed reaction sequence excludes promotion by adsorbed O atoms.

In regard to step {6}, it has been proposed that either hydroxyl groups (10) or O atoms (15, 25, 60) react with surface CH_x fragments; however, because the reaction of CH_x with either adsorbed O or OH does not change the mathematical form of the derived rate expression, exclusion of either species as the intermediate oxidant is not possible on the basis of kinetic data alone. In a study of CH_4 partial oxidation and mixed CO_2/H_2O–CH_4 reforming, Qin *et al*. correlated CO formation rates with the metal–oxygen bond strength of adsorbed O atoms, as estimated by the heat of formation of the most stable oxide (25); however, because these authors did not use specific activities in their correlation, the validity of their correlation is very questionable. In addition, such a correlation does not prove that adsorbed oxygen atoms are a key reaction intermediate because the binding energies for O and OH on transition metal surfaces are directly proportional (59, 61, 62). Shustorovich and Bell have calculated the activation barriers for two elementary steps—$C* + OH* \rightarrow CO* + H*$ and $C* + O* \rightarrow CO*$—on Pt(111) to be 0 and 6 kcal/mol, respectively (61), thus providing further support for assuming that adsorbed CH_x fragments preferentially react with OH groups, as shown in step {6}, over supported Pt catalysts.

Several investigations have probed the rate-determining steps of CO_2–CH_4 reforming. Wang and Au recently used CD_4 to find a kinetic isotope effect with Ni/SiO_2 and concluded that CH_4 dissociation is rate determining and CO_2 dissociation occurs prior to the surface reaction of CH_x fragments (60). The observation by Zhang and Verykios that the CH_4/CD_4 isotope effect over Ni/La_2O_3 and Ni/γ-Al_2O_3 decreases with increasing temperature (63) is consistent with molecular beam results for CH_4 and CD_4 adsorption on transition metal surfaces which have shown that the apparent activation energy for CD_4 dissociation is typically higher than that for CH_4 (64). In addition, the weak isotope effect observed by Zhang and Verykios over Ni/γ-Al_2O_3 (63) may be due to the Ni crystallite structure; i.e., molecular beam studies have shown that while a strong CH_4/CD_4 isotope effect exists on both the Ni(111) (65) and Ni(100) surfaces (66), there is virtually no isotope effect on Ni(110) (66). Osaki *et al*. employed pulsed surface reaction analysis (PSRA) and concluded that two reaction steps are responsible for H_2 production, i.e., dissociative CH_4 adsorption to form CH_x species and the subsequent surface reaction of CH_x, and that the surface reaction of CH_x and O is rate determining (58). Nevertheless, the choice of reaction steps {1} and {7} as the slow kinetic steps in the proposed reaction sequence is further supported by activation energies reported for analogous homogeneous gas-phase reactions (10). The reactions between CH_x and OH occur in the gas phase with no activation barrier, i.e., they are facile, free radical reactions, and activation barriers for OH formation and the reaction of CH_x with O atoms in the gas phase are also zero (67). Thus, it seems more plausible that CH_xO decomposition, rather than the reaction of two radical species, such as CH_x with O (or OH), is rate determining. Because a surface reaction between CH_x and O (or OH) is difficult to differentiate from the decomposition of a subsequently formed CH_xO intermediate on the basis of isotope effects and PSRA alone, the results of Wang and Au (60), Zhang and Verykios (63), and Osaki *et al*. (58) are not inconsistent with the choice of CH_4 dissociation and CH_xO decomposition as slow kinetic steps in our kinetic model.

Reaction steps {2}–{5} and {8} represent the RWGS reaction and are assumed to be quasi-equilibrated to accommodate the experimental result that this reaction is near thermodynamic equilibrium (Fig. 9). Rostrup-Nielsen and Bak

Hansen have shown that the RWGS is more than 20 times more rapid, on a TOF basis, than CO_2–CH_4 reforming over 0.9% Pt/MgO (23). Nondissociative adsorption of CO_2 under reaction conditions is assumed to occur on the support in the form of carbonates, as evidenced by the *in situ* DRIFT spectra shown in Fig. 11. H-assisted carbonate dissociation has been discussed previously (10) and is further evidenced by the TPH results shown in Fig. 5. On Pt/TiO_2, reaction steps {2}–{4} may involve a type of redox cycle, as previously suggested by DRIFTS and TPSR results. Otsuka *et al*. have provided evidence to indicate that a redox reaction may occur during CO_2 reforming of CH_4 over Pt/CeO_2 (27).

In view of the aforementioned discussion, the proposed reaction mechanism for CO_2 reforming of CH_4 over supported Ni should be applicable to supported Pt catalysts. If it is assumed as before (10) that the most abundant reaction intermediate (mari) is CH_xO, then $L = [*] + [CH_xO*]$ and the following general expression may be derived for the rate of CH_4 consumption:

$$r_{CH_4} = \frac{\hat{k}_1 P_{CH_4} P_{CO_2}}{(\hat{k}_{-1}\bar{K}/\hat{k}_7) P_{CO} P_{H_2}^{(4-x)/2} + (1 + (\hat{k}_1/\hat{k}_7) P_{CH_4}) P_{CO_2}}. \quad [9]$$

Here, $\hat{k}_i = k_i L$, L = total number of active sites, and $\bar{K}$ is a lumped equilibrium constant (10). Computer optimization of kinetic data from the Pt/TiO_2 catalyst failed to locate a global minimum for x and indicated that the statistical fit of the data (as measured by residual sum of squares) of Eq. [9] was essentially independent of x ($0 \le x \le 4$). A value of $x = 0$ would physically imply that adsorbed C atoms are the active CH_x intermediate and adsorbed CO is the mari; however, inclusion of adsorbed CO in the site balance did not improve the statistical fit of the model. In view of the aforementioned discussion, it is very possible that a distribution of CH_x species exists under reforming conditions; thus, for simplicity the partial pressure data for Pt/TiO_2 were optimized to Eq. [9] by assuming an arbitrary but reasonable value of $x = 2$. The recent identification of a CH_2O surface species supports this choice (68). The results are shown in Fig. 14, and values of the optimized model parameters are provided in Table 6.

Plots of these model parameters versus reciprocal temperature yielded the activation energy for step {1} in the forward direction, $E_{\hat{k}_1}$, the activation energy for step {7}, $E_{\hat{k}_7}$, and a lumped energy parameter, $-(E_{\hat{k}_{-1}} + \Delta H_{\bar{K}})$, where $E_{\hat{k}_{-1}}$ is the activation energy for step {1} in the reverse direction, and $\Delta H_{\bar{K}}$ is the enthalpy change for a lumped reaction (10). The activation energies in Table 7 obtained with the model can be compared with literature values for similar, but not identical reactions on Pt(111) (62, 69, 70). Although these values are not widely divergent, they support the proposal that the reaction is not occurring solely on the Pt surface, but primarily in the metal–support interfacial region. Considering that TiO_x species are decorating the Pt surface and that CH_xO species most likely are formed and subsequently decomposed at the metal–support interface, this suggestion is not unreasonable. As a test of the optimized model parameters in Tables 6 and 7, the activity of Pt/TiO_2 was measured at 883 K using a feed ratio of $CH_4/CO_2/He = 1/3.7/4.9$ and compared with that predicted using Eq. [9]. Although the initial rate of CH_4 disappearance was about 20% higher than that predicted, the rate was

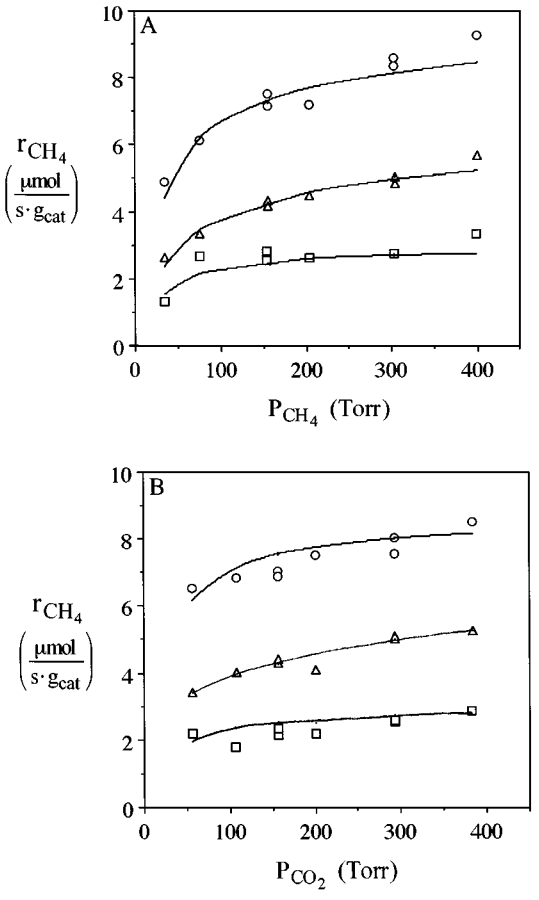

FIG. 14. Fit of the kinetic model for Pt/TiO_2 as a function of (A) CH_4 partial pressure and (B) CO_2 partial pressure at (□) 673 K, (△) 698 K, and (○) 723 K.

TABLE 6

Optimized Kinetic Model Parameters for Pt/TiO_2 Using $x = 2$

T (K)	Parameter		
	$\hat{k}_1$ [a,b]	$\hat{k}_7$ [c]	$\hat{k}_{-1}\bar{K}$ [b]
673	0.099 ± 0.099	3.36	37.3
698	0.117 ± 0.034	7.40	24.1
723	0.265 ± 0.116	10.35	9.09

[a] Value is reported ±95% confidence interval.
[b] Units of μmol g cat^{-1} s^{-1} $Torr^{-1}$.
[c] Units of μmol g cat^{-1} s^{-1}.

TABLE 7

Energetic Parameters from the Kinetic Model and the Literature

Surface reaction	E (kcal/mol) Pt/TiO_2[a]	E (kcal/mol) Pt(111)
$CH_4 + * \xrightarrow{\hat{k}_1} CH_2* + H_2$	19	
$CH_4 + 2* \rightarrow CH_3* + H*$		12[b], 29[c]
$CH_2O* \xrightarrow{\hat{k}_7} CO* + H_2$	22	
$CH_2O* + * \rightarrow HCO* + H*$		11[b]
$CH_2O* + 2* \rightarrow CO* + 2H*$		13.4[d]

[a] From kinetic parameters in Table 6.
[b] Shustorovich (62).
[c] Zaera (69).
[d] Sun and Weinberg (70).

within 5% of the predicted value after about 5 h onstream (44).

The reasons for the stability of Pt/ZrO_2 are possibly due to strong $Pt–Zr^{n+}$ interactions which may block Lewis acid sites on the support, alter Pt morphology, and form ZrO_x species on the Pt surface. Although the role of ZrO_2 at the metal–support interface may also be to provide lattice oxygen species that participate in the reaction mechanism, as shown by Efstathiou *et al*. using transient methods and isotopically labeled $C^{18}O_2$ (71), the insignificant differences in the specific activities of Pt/ZrO_2, Pt/Cr_2O_3, and Pt/SiO_2 would imply that the role of any lattice oxygen species is minor. However, these species may play a role in the minimization of carbon deposition on the Pt surface under reaction conditions.

SUMMARY

The support was shown to play a major role in decreasing carbon deposition and a much lesser role in determining activity in the $CO_2–CH_4$ reforming reaction over Pt. The apparent absence of any significant metal–support interaction in Pt/SiO_2 and Pt/Cr_2O_3 resulted in substantial carbon deposition and rapid deactivation. Dispersing Pt on TiO_2 resulted in suppression of carbon deposition, presumably due to an ensemble effect created by TiO_x species migrating onto the Pt surface, whereas the suppression of carbon deposition on Pt/ZrO_2 may be due to the consequence of an interaction of Pt with Zr^{n+} centers, the participation of lattice oxygen species at the metal–support interface, or partial coverage of Pt by ZrO_x species, as occurs with titania. The predominant reason is unclear at this time. The influence of the support on catalyst activity is multifaceted and appears to involve the adsorption and subsequent activation of CO_2 via the RWGS, a role as a reservoir for surface hydroxyl groups, and the formation and subsequent decomposition of CH_xO species, presumably in the metal–support interfacial region; regardless, TOFs on four different catalysts varied by only a factor of 5. A reaction model invoking dissociative CH_4 adsorption and CH_xO decomposition as slow kinetic steps successfully correlated all kinetic data.

ACKNOWLEDGMENTS

The authors thank a Japanese international joint research program, NEDO, for sponsoring this study, the U.S. Department of Education for providing a GAANN fellowship, Professor J. Lercher and his group for providing the Pt/ZrO_2 catalyst, Professor J. H. Lunsford and his group for providing laser Raman analysis of the Pt/ZrO_2 catalyst, and Professor R. T. K. Baker and his group for determining the pore size distributions. The DRIFTS system was purchased with funds provided by an NSF equipment grant (CTS-9311087).

REFERENCES

1. Gadalla, A. M., and Bower, B., *Chem. Eng. Sci.* **43**, 3049 (1988).
2. McCrary, J., McCrary, G. E., Chubb, T. A., Nemecek, J. J., and Simmons, D. E., *Sol. Energy* **29**, 141 (1982).
3. Edwards, J. H., Do, K. T., Maitra, A. H., Schuck, S., and Stein, W., *Sol. Eng.* **1**, 389 (1995).
4. Fish, J. D., and Hawn, D. C., *J. Sol. Energy Eng.* **109**, 215 (1987).
5. Delmon, B., *Appl. Catal. B Environ.* **1**, 139 (1992).
6. Teuner, S., *Hydrocarbon Process.* **66**, 52 (1987).
7. Udengaard, N. R., Hansen, J-H. B., and Hanson, D. C., *Oil Gas J.* **90**, 62 (1992).
8. Tokunaga, O., and Ogasawara, S., *React. Kinet. Catal. Lett.* **39**, 69 (1989).
9. Guerrero-Ruiz, A., Sepúlveda-Escribano, A., and Rodríguez-Ramos, I., *Catal. Today* **21**, 545 (1994).
10. (a) Bradford, M. C. J., and Vannice, M. A., *Appl. Catal.* **142**, 73 (1996); (b) Bradford, M. C. J., and Vannice, M. A., *Appl. Catal.* **142**, 97 (1996).
11. Basini, L., and Sanfilippo, D., *J. Catal.* **157**, 162 (1995).
12. Zhang, Z. L., Tsipouriari, V. A., Efstathiou, A. M., and Verykios, X. E., *J. Catal.* **158**, 51 (1996).
13. Erdöhelyi, A., Cserényi, J., Papp, E., and Solymosi, F., *Appl. Catal. A Gen.* **108**, 205 (1994).
14. Perera, J. S. H. Q., Couves, J. W., Sankar, G., and Thomas, J. M., *Catal. Lett.* **11**, 219 (1991).
15. Solymosi, F., Kutsán, Gy., and Erdöhelyi, A., *Catal. Lett.* **11**, 149 (1991).
16. Sakai, Y., Saito, H., Sodesawa, T., and Nozaki, F., *React. Kinet. Catal. Lett.* **24**, 253 (1984).
17. Tokunaga, O., Osada, Y., and Ogasawara, S., *Fuel* **68**, 990 (1989).
18. Vernon, P. D. F., Green, M. L. H., Cheetham, A. K., and Ashcroft, A. T., *Catal. Today* **13**, 417 (1992).
19. Masai, M., Kado, H., Miyake, A., Nishiyama, S., and Tsuruya, S., *in* "Methane Conversion" (D. M. Bibby, C. D. Chang, R. F. Howe, and S. Yurchak, Eds.), p. 67. Elsevier Science, Amsterdam, 1988.
20. Gustafson, B. L., and Walden, J. V., U.S. Patent No. 5,068,057.
21. Seshan, K., ten Barge, H. W., Hally, W., van Keulen, A. N. J., and Ross, J. R. H., *in* "Natural Gas Conversion II" (H. E. Curry-Hyde and R. F. Howe, Eds.), p. 285. Elsevier, Amsterdam, 1994.
22. Bitter, J. H., Hally, W., Seshan, K., van Ommen, J. G., and Lercher, J. A., *Catal. Today* **29**, 349 (1996).
23. Rostrup-Nielsen, J. R., and Bak Hansen, J-H., *J. Catal.* **144**, 38 (1993).
24. Qin, D., and Lapszewicz, J., *Catal. Today* **21**, 551 (1994).
25. Qin, D., Lapszewicz, J., and Jiang, X., *J. Catal.* **159**, 140 (1996).
26. Moene, R., Ph.D. dissertation (ISBN No. 90-407-1109-7), Delft University of Technology, 1995.
27. Otsuka, K., Ushiyama, T., and Yamanaka, I., *Chem. Lett.* 1517 (1993).
28. Inui, T., *in* "New Aspects of Spillover Effect in Catalysis" (T. Inui, K. Fujimoto, T. Uchijima, and M. Masai, Eds.), p. 17. Elsevier, Amsterdam, 1993.

29. Kim, G. J., Cho, D.-S., Kim, K.-H., and Kim, J.-H., *Catal. Lett.* **28**, 41 (1994).
30. Yu, Z., Choi, K., Rosynek, M. P., and Lunsford, J. H., *React. Kinet. Catal. Lett.* **51**, 143 (1993).
31. Tauster, S. J., *Acc. Chem. Res.* **20**, 389 (1987).
32. Yates, D. J. C., and Sinfelt, J., *J. Catal.* **8**, 348 (1967).
33. Peters, J. A., "ARL Technical Report 88-008," Pennsylvania State University, 1988.
34. Guglielminotti, E., *Langmuir* **6**, 1455 (1990).
35. Jacob, K.-H., Knözinger, E., and Benfer, S., *J. Mater. Chem.* **3**, 651 (1993).
36. Davydov, A. A., Komarova, M. P., Anufrienko, V. F., and Maksimov, N. G., *Kinet. Catal.* **14**, 1342 (1973).
37. Baker, R. T. K., Prestridge, E. B., and Garten, R. L., *J. Catal.* **56**, 390 (1979).
38. Hadjiivanov, K., and Busca, G., *Langmuir* **10**, 4534 (1994).
39. Weisz, P., *Z. Phys. Chem. N.F.* **11**, 1 (1957).
40. (a) Vannice, M. A., and Twu, C. C., *J. Catal.* **82**, 213 (1983); (b) Vannice, M. A., *J. Catal.* **74**, 199 (1982).
41. Davydov, A. A., "Infrared Spectroscopy of Adsorbed Species on the Surface of Transition Metal Oxides." Wiley, Chichester/New York, 1990.
42. Kondo, J., Abe, H., Sakata, Y., Marayu, K.-I., Domen, K., and Onishi, T., *J. Chem. Soc. Faraday Trans. 1* **84**, 511 (1988).
43. Sanz, J., Rojo, M., Malet, P., Munuera, G., Blasco, M. T., Conesca, J. C., and Soria, J., *J. Phys. Chem.* **89**, 5427 (1985).
44. Bradford, M. C. J., Ph.D. dissertation, Pennsylvania State University, 1997.
45. Fancheng, W., Huilin, W., Tsai, K. R., Shuijuand, W., and Fuchun, X., *Catal. Lett.* **12**, 319 (1992).
46. Sankar, G., Kannan, K. R., and Rao, C. N. R., *Catal. Lett.* **8**, 27 (1991).
47. Van Santen, R. A., and Neurock, M., *Catal. Rev. Sci. Eng.* **37**, 557 (1995).
48. Zhang, Z., and Verykios, X. E., *Appl. Catal. A Gen.* **138**, 109 (1996).
49. Minot, C., van Hove, M. A., and Somorjai, G. A., *Surf. Sci.* **127**, 441(1982).
50. Koster, A. D. E., and van Santen, R. A., *J. Catal.* **127**, 141 (1991).
51. Van Keulen, A. N. J., Ph.D. dissertation (ISBN No. 90-9009877-1), University of Twente, 1996.
52. Roberts, S., and Gorte, R. J., *J. Phys. Chem.* **95**, 5600 (1991).
53. Yamazaki, O., Nozaki, T., Omata, K., and Fujimoto, K., *Chem. Lett.* **10**, 1953 (1992).
54. Philipp, R., and Fujimoto, K., *J. Phys. Chem.* **96**, 9035 (1992).
55. Mark, M. F., and Maier, W. F., *Angew. Chem. Int. Ed. Eng.* **33**, 1667 (1994).
56. Kroll, V. C. H., Delichure, P., and Mirodatos, C., *Kinet. Catal.* **37**, 698 (1996).
57. Kroll, V. C. H., Swaan, H. M., and Mirodatos, C., *J. Catal.* **161**, 409 (1996).
58. Osaki, T., Horiuchi, T., Suzuki, K., and Mori, T., *J. Chem. Soc. Faraday Trans.* **92**, 1627 (1996).
59. Shustorovich, E., and Bell, A. T., *Surf. Sci.* **268**, 397 (1992).
60. Wang, H.-Y., and Au, C.-T., *Catal. Lett.* **38**, 77 (1996).
61. Shustorovich, E., and Bell, A. T., *Surf. Sci.* **248**, 359 (1991).
62. Shustorovich, E., *Adv. Catal.* **37**, 101 (1990).
63. Zhang, Z., and Verykios, X. E., *Catal. Lett.* **38**, 175 (1996).
64. Luntz, A. C., and Harris, J., *Surf. Sci.* **258**, 397 (1991).
65. Ceyer, S. T., Yang, Q. Y., Lee, M. B., Beckerle, J. D., and Johnson, A. D., *in* "Methane Conversion" (D. M. Bibby, C. D. Chang, R. F. Howe, and S. Yurchak, Eds.), p. 51. Elsevier, Amsterdam, 1988.
66. Beebe, T. P., Jr., Goodman, D. W., Kay, B. D., and Yates, J. T., Jr., *J. Chem. Phys.* **87**, 23105 (1987).
67. Miller, J. A., and Bowman, C. T., *Prog. Energy Comb. Sci.* **15**, 287 (1989).
68. Bradford, M. C. J., and Vannice, M. A., submitted for publication.
69. Zaera, F., *Catal. Lett.* **11**, 95 (1991).
70. Sun, Y.-K., and Weinberg, W. H., *Surf. Sci.* **227**, L86 (1990).
71. Efstathiou, A. M., Kladi, A., Tsipouriari, V. A., and Verykios, X. E., *J. Catal.* **158**, 64 (1996).